

DA-BEV : Depth Aware BEV Transformer for 3D Object Detection

Hao Zhang^{1,4*} Hongyang Li^{2,4} Xingyu Liao³ Feng Li^{1,4} Shilong Liu^{5,4}
Lionel M. Ni⁶ Lei Zhang^{4†}

¹The Hong Kong University of Science and Technology.

²South China University of Technology.

³University of Science and Technology of China

⁴International Digital Economy Academy (IDEA).

⁵Dept. of CST., BNRist Center, Institute for AI, Tsinghua University.

⁶The Hong Kong University of Science and Technology (Guangzhou).

Abstract

In this paper, we present DA-BEV, an implicit depth learning method for Transformer-based camera-only 3D object detection in bird's eye view (BEV). First, a Depth-Aware Spatial Cross-Attention (DA-SCA) module is proposed to take depth into consideration when querying image features to construct BEV features. Then, to make the BEV feature more depth-aware, we introduce an auxiliary learning task, called Depth-wise Contrastive Learning (DCL), by sampling positive and negative BEV features along each ray that connects an object and a camera. DA-SCA and DCL jointly improve the BEV representation and make it more depth-aware. We show that DA-BEV obtains significant improvement (+2.8 NDS) on nuScenes val under the same setting when compared with the baseline method BEVFormer. DA-BEV also achieves strong results of 60.0 NDS and 51.5mAP on nuScenes test with pre-trained VoVNet-99 as backbone. We will release our code after blind review.

1. Introduction

3D object detection is a fundamental task for many applications such as autonomous driving and robotics. Recently, camera-based 3D perception has attracted great attention from both academia and industry. Different from LiDAR-based methods, camera-based methods have advantages such as low cost, long perception range, and the ability to identify vision-only signals such as traffic lights and stop signs. One key challenge for camera-based methods is the lack of depth information. Previous works [13, 19] have proved that high-quality depth can remarkably help improve 3D detection performance. Although many works are trying to

recover depth from camera images, depth estimation is still an ill-posed problem.

Some works explicitly estimate depth and then use the predicted depth for downstream tasks. For example, a branch of research [26, 28, 29] utilizes a stand-alone depth estimation network to output depth maps and generates pseudo-LiDAR information from the depth maps. After pseudo-LiDAR information is generated, a LiDAR-based detector can be used for 3D detection. Such works depend on a depth network to generate high-quality pseudo-LiDAR information. Therefore, their performance is greatly constrained by the depth estimation quality and thus subjects to compounding errors [27]. Some researchers [4, 22] also find this paradigm sub-optimal due to non-differentiable transformation from 2D to 3D space. Recently, BEVDepth [13] proposes to supervise depth learning with LiDAR-generated sparse depth labels. It also leverages camera information for more precise depth estimation and proposes a depth correction module to reduce error from disturbance of camera extrinsics. BEVDepth obtains a strong performance due to the high quality of depth it estimates.

Another line of works directly predicts 3D boxes without predicting depth. For instance, researchers [33] find that CenterNet can be used to predict 3D boxes by changing the box head slightly. FCOS3D [25] transforms 3D targets to the image domain and decouples them as 2D and 3D attributes. This line of works can be viewed as learning depth implicitly by predicting 3D locations of object boxes. Recently, motivated by DETR-based models for 2D object detection, some DETR-based 3D detectors are proposed [14, 16, 27]. They also belong to this category of works. Although they are among the top performed camera-based 3D detectors, they have a common problem when using object queries to probe image features. The problem is due to that they con-

*This work was done when Hao Zhang was an intern at IDEA.

†Corresponding author.

duct Spatial Cross-Attention (SCA)¹ in a way that is naively inherited from 2D detection without considering the intrinsic characteristic in 3D space. Concretely, they only take (u, v) ² into consideration but ignore a very important information d . Without depth, their approach is conceptually indirect and inefficient for the detection head to distinguish the depths of different objects. In consequence, an ambiguity problem (see Section 3.1) will occur which may lead to duplicate predictions along depth axes.

To solve the problem, we present a novel improvement by introducing depth into the Spatial Cross-Attention (SCA) module. For each BEV query³, when probing features from a camera view, we let its positional part be the positional encoding of (u, v, d) converted from its 3D reference point (x, y, z) according to the BEV-to-camera transformation matrix. We also add (u, v, d) encoding to image features, where d is predicted from image features. We show that simply adding depth encoding effectively improves the detection performance. To further make BEV features depth-aware, a Depth-wise Contrastive Learning (DCL) approach is also proposed to help the network learn depth-aware BEV features in an implicit way. More specifically, we sample positive and negative BEV features along a ray from a camera to an object center, which is denoted as an object ray, as shown in Fig. 1. A BEV feature is considered positive if it is close (within a predefined scope) to an object center and negative otherwise. After that, an auxiliary contrastive loss is applied to the sampled BEV features in the training phase, where positive features are expected to predict objects and negative ones are expected to predict “no object”. Such an auxiliary task effectively encourages the network to learn a depth-aware BEV representation by working with the DA-SCA module.

In summary, our contributions are three-fold. First, we propose a Depth-Aware Spatial Cross-Attention (DA-SCA) module which includes depth information in both query and value when querying image features. Second, based on DA-SCA, we propose a Depth-wise Contrastive Learning (DCL) method for implicit depth learning, which improves the performance significantly. Third, when evaluating our proposed method on nuScenes dataset, we obtain 54.5 NDS with ResNet101 as backbone which is +2.8 NDS higher than our baseline BEVFormer. We also achieve 60.0 NDS with VoVNet-99 [19] pre-trained on dense depth estimation task as backbone which is a SOTA result under the same backbone.

¹We follow BEVFormer to call the cross attention that probe image features to Bird Eye View(BEV) features as Spatial Cross-Attention.

²By default, we use (u, v, d) to denote coordinates in a camera coordinate system, where (u, v) are the 2d coordinates in an image plane and d is the depth whose direction is perpendicular to the image plane. We also use (x, y, z) to denote coordinates in an ego vehicle coordinate system.

³We follow BEVFormer to use BEV queries.

2. Related Work

Depth learning in camera-based 3D detection: Camera-based 3D detection requires predicting 3D boxes only from camera data, in which depth learning is the most challenging because it is an ill-posed problem. One line of works predicts depth explicitly and then uses depth for 3D detection. These works can be divided into two categories [21]: result-lifting methods and feature-lifting methods. Result-lifting methods [3, 10, 12, 18, 23] break down 3D detection into 2D detection and depth prediction and predict objects according to geometric properties and constraints. These methods severely rely on feature engineering which hinders them from generalizing to various scenarios. Feature lifting methods lift image features into 3D space. Some [20, 26, 31] predict depth map from image features and then lift the depth map into pseudo-LiDAR to mimic LiDAR signal. Once the pseudo-LiDAR signal is generated, they can utilize a LiDAR-based detection head for detection. Some learn a categorical depth distribution [13, 22] and then project image features into 3D space [22] or BEV plane [13]. BEVDepth [13] supervises depth learning with sparse LiDAR data and proposes a depth correction module to reduce depth error. Their method establishes a new SOTA result on nuScenes 3D detection task with camera data only. The explicit depth learning methods require a depth network and ground truth depth labels. Another branch of research learn depth implicitly. For example, DETR3D uses object queries to probe features and output a prediction for each query without predicting depth. **DETR-based 3D detectors:** Recently, DETR-based models [2, 11, 15, 32, 35] have achieved great success in 2D detection. The core of the DETR-based models is to query image features with some object queries, which is called Spatial Cross-Attention (SCA) in this paper. The first DETR-based model on nuScenes detection task is DETR3D [27]. It contains a feature extractor and a detection head. The detection head converts 3D reference points into camera reference points and then uses single-point deformable attention to probe image features. PETR [16] is also a simple DETR framework for 3D detection. It adopts standard attention that uses the relativity of key and query to guide feature probing. Instead of mapping 3D reference points to 2D reference points in the camera plane, it lifts the camera plane into 3D space along depth axes. Because an image feature only has camera coordinates (u, v) and does not contain depth. It samples depths with equal space in a valid scope denoted as d_1, d_2, \dots, d_k . For each depth d_i , it converts (u, v, d_i) into 3D coordinates (x_i, y_i, z_i) . The positional encoding of the key is the sum over positional encodings of all (x_i, y_i, z_i) for i from 1 to k . Therefore, the key and query are aligned in an ego-vehicle coordinate system. Another work BEVFormer [14] is similar to DETR3D, converting 3D reference points into camera reference points. Differently, it uses BEV queries to map image features into BEV plane and utilizes an

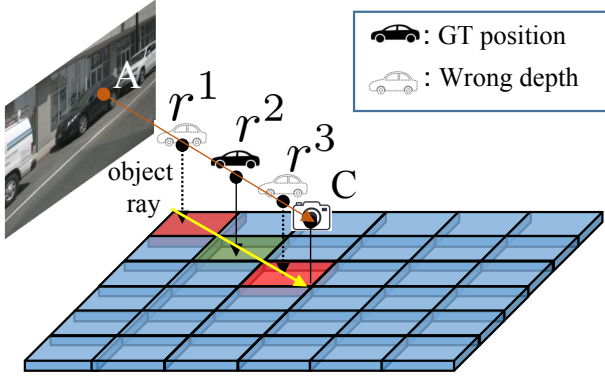


Figure 1. An illustration of a common ambiguity problem in DETR-based 3D detectors. AC is a ray pointing from an object center A to a camera C . The yellow ray is the projection of the object ray AC on the BEV plane. Note that 3D reference points r^1 , r^2 , and r^3 will be mapped to the same camera reference point. The car drawn with a solid line at r^2 denotes the GT center of the object, whereas the ones with dash lines at r^1 and r^3 means the object is not in these positions, but detection head will “see” an object there. The green cell denotes the BEV feature at the GT center and the red cells denote BEV features at pseudo-GT centers.

extra detection head to predict boxes. In summary, DETR3D and BEVFormer map 3D reference points into camera plane without using depth information. PETR lifts image features along depth axes, but it does not have a bias on depths.

3. Method

3.1. Motivation

The initial motivation of our method comes from a common problem in the design of previous DETR-base 3D detectors. In Fig.1, we take BEVFormer as an example to illustrate the problem. Assuming that there is an object ray from A to C and there are three 3D reference points r^1 , r^2 , and r^3 along the ray with three corresponding BEV features q^1 , q^2 , and q^3 . We assume that object center is exactly located at r^2 . Denote $r^i = (x^i, y^i, z^i)$. In the Spatial Cross-Attention module of BEVFormer, r^i is mapped to a camera reference point (u^i, v^i) on a camera plane. (u^i, v^i) is then treated as a 2D reference point for deformable attention. Since r^1 , r^2 , and r^3 are all on the ray AC , we have $(u^1, v^1) = (u^2, v^2) = (u^3, v^3)$. Therefore, the queries in different 3D locations such as q^1 , q^2 , and q^3 will probe image features based on the same camera reference point. This ambiguity makes it hard for the detection head to tell where the object is exactly located, particularly along the depth direction. This problem may also cause duplicate prediction because BEV features probed by q^1 , q^2 , and q^3 all contains the feature of the object. We argue that this is a common problem in current DETR-based 3D detectors, not only in BEVFormer, but also in DETR3D [27] and PETR [16], be-

cause they all query image features in a similar manner.

An intuitive solution to address this ambiguity issue is to obtain a depth information for the image feature at (u^1, v^1) ⁴ and compare it with the depth information of r^1 , r^2 and r^3 , so that for different BEV queries q^1 , q^2 , and q^3 , the image feature at (u^1, v^1) augmented with the depth information will contribute differently to different BEV queries. This comparison requires depth information for both BEV features and image features. Therefore, we propose a Depth-Aware Spatial Cross-Attention (DA-SCA) module to include depth information in both BEV queries and image features when querying features. To further make BEV features depth-aware, a novel Depth-wise Contrastive Learning (DCL) is also proposed which boosts the learning of depth and comparison at the same time. More details are described in Section 3.3 and 3.4.

3.2. Overview

As shown in Fig. 2, our training pipeline can be divided into four parts. The feature extractor takes multi-view images as input and output image features and positional encodings, which will be used by the BEV encoder. Similar to BEVFormer, our BEV encoder includes a Temporal Self-Attention (TSA) module and a Spatial Cross-Attention (SCA) module in each layer. TSA is performed over BEV features of adjacent frames to capture object motion information. In SCA, BEV queries probe image features through deformable cross-attention. In this paper, we mainly focus on the problem of lacking depth information in SCA. Therefore, we include depth encoding in both queries and values. After BEV Encoder, the output of BEV features are used to conduct depth-wise contrastive learning. Instead of random sampling, we find that sampling positive and negative examples along object rays introduces a great improvement in depth learning. Note that depth-wise contrastive learning is only used during training and will not add any inference overhead. Finally, the BEV features are fed to the detection head to predict 3D bounding boxes and their object classes. In this work, we use deformable DETR [35] as the detection head.

3.3. Depth-Aware Spatial Cross-Attention

Previous DETR-based 3D detectors neglect depth when performing Spatial Cross-Attention (SCA), while we give it a thorough consideration in this work. Fig. 3 shows a comparison between our Depth-Aware SCA (DA-SCA) and SCA in previous methods. PETR uses Positional Encoding (PE) of (x, y, z) coordinates, which are called 3D PE here, in queries and keys. The positional query is the sine positional encoding [24] of learnable 3D reference points. To align with query, their positional key should also be PE of (x, y, z) coordinates. Since the conversion from a camera coordinate

⁴We have $(u^1, v^1) = (u^2, v^2) = (u^3, v^3)$.

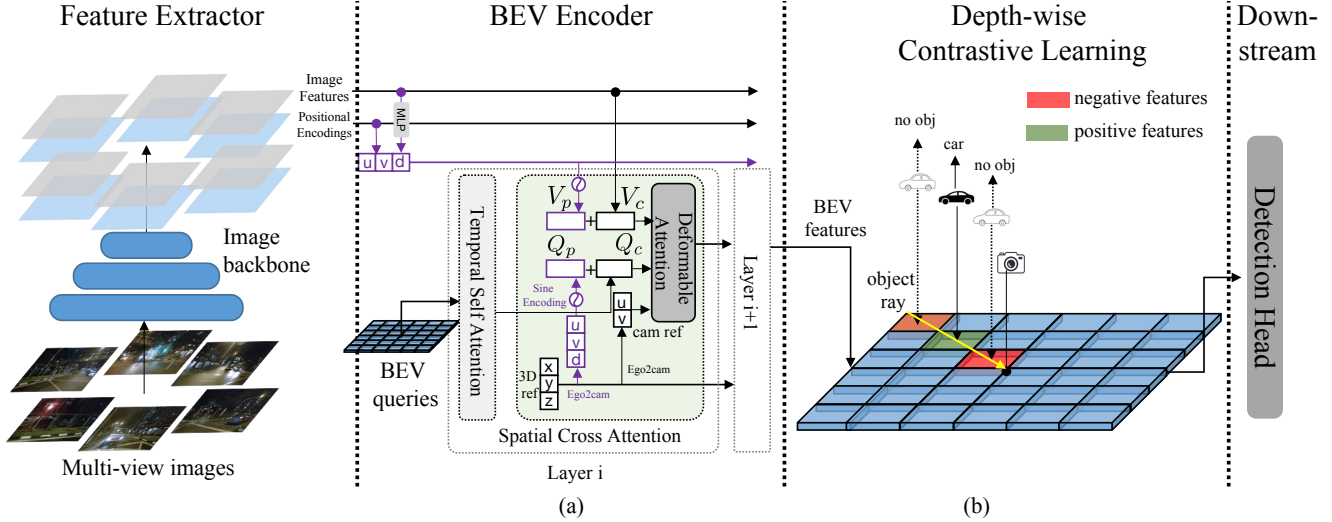


Figure 2. The training pipeline of our method. It contains four parts: feature extractor, BEV encoder, Depth-wise Contrastive Learning (DCL), and the downstream task. (a) A BEV encoder layer contains a Temporal Self-Attention (TSA) module and a Spatial Cross-Attention (SCA) module. Our SCA is a deformable attention with three inputs: a value V , a query Q , and a camera reference point (u, v) . The Q and V both have a content part Q_c and V_c and a positional part Q_p and V_p . “3D ref” and “cam ref” denote a 3D reference point in the ego-vehicle coordinate system and a 2D reference point in a camera coordinate system. “Ego2cam” denotes the transformation from the ego-vehicle coordinate system to the camera coordinate system. (b) The yellow ray on the BEV features is named as an object ray which connects the center of an object and a camera. The object ray passes through several BEV queries: the red ones denote two negative features and the green one denotes a positive feature.

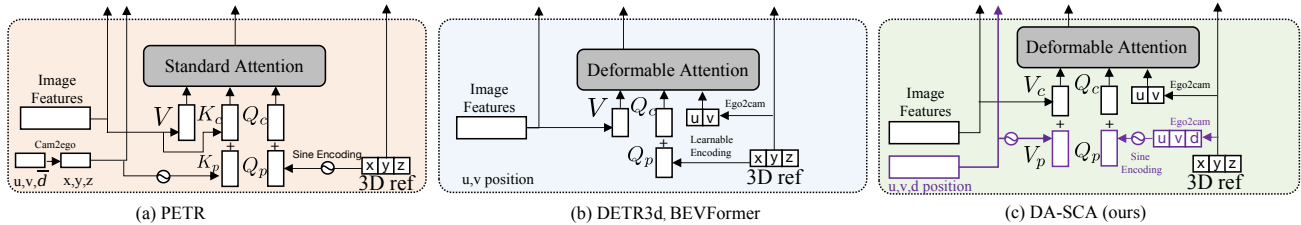


Figure 3. The comparison between DA-SCA and SCA in previous works. PETR adopts standard attention. They include positional encoding of (x, y, z) in both queries and keys. For keys, they do not have d , so they sample d uniformly along the depth direction in a valid scope and sum up all the positional encodings of converted (x, y, z) over all d 's, we use \bar{d} to indicate that they do not have informative depth. DETR3D and BEVFormer adopt deformable attention without using keys. They use a (u, v) reference point to guide where to query features from and add positional encoding of (x, y, z) to the content part of a query for predicting deformable sampling points. They all neglect the depth information in SCA. By contrast, DA-SCA adopts (u, v, d) positional encoding in both image features and queries.

system to the ego-vehicle coordinate system needs depth information for each pixel at (u, v) , they uniformly sample several depths within a valid scope denoted as d_1, d_2, \dots, d_n and obtain (x_i, y_i, z_i) for each (u, v, d_i) . The PE of the pixel at (u, v) is then computed as $\sum_i \text{PE}(x_i, y_i, z_i)$. Although PETR introduces depth into SCA, its uniform depth sampling mechanism does not bring in useful depth information in SCA. DETR3D [27] and BEVFormer adopt deformable attention⁵, which do not use keys for SCA. They both adopt 3D PE as the positional queries and do not have positional

⁵The implementation of SCA in DETR3D is a single-point deformable attention which only queries features at a reference point. Here we regard DETR3D as a special case of BEVFormer in terms of deformable attention.

values. The main problem lies in the sharing of camera reference points for all BEV features along an object ray as revealed in Fig. 1. Moreover, for a BEV query, BEVFormer predicts sampling points based on its 3D PE and will lead to the same sampling points for different camera views, which is not a plausible assumption.

To clarify our Depth-Aware SCA (DA-SCA), we denote a 3D reference point as (x, y, z) . An image feature at (u_c, v_c) is taken as the content value V_c and a depth map \mathbf{d} is predicted from the image feature map. The positional query Q_p

can be calculated as follows.

$$\begin{aligned} u, v, d &= \text{Ego2cam}(x, y, z) \\ Q_p &= \text{SinePE}(u, v, d), \end{aligned} \quad (1)$$

where Ego2cam is the transformation from the ego-vehicle coordinate system to a camera coordinate system and SinePE is the sine positional encoding function. The positional value Q_p can be obtained as follows.

$$V_p = \text{SinePE}(u_c, v_c, \mathbf{d}[u_c, v_c]), \quad (2)$$

where $\mathbf{d}[u_c, v_c]$ means to take the value of \mathbf{d} at (u_c, v_c) . The relation between the input and output of DA-SCA can be written as follows.

$$\begin{aligned} F &= \text{DeformAttn}(Q, r, V) \\ &= \text{DeformAttn}(Q_c + Q_p, r, V_c + V_p) \\ &= \text{DeformAttn}(Q_c + \text{SinePE}(u, v, d), (u, v), \\ &\quad V_c + \text{SinePE}(u_c, v_c, \mathbf{d}[u_c, v_c])) \end{aligned} \quad (3)$$

Because there is a residual connection between input queries and output features, the output features contain the information of d and $\mathbf{d}[u_c, v_c]$, which can be used to distinguish if their depths are matched, therefore resolving the ambiguity illustrated in Fig. 1.

3.4. Depth-wise Contrastive learning

Given that we have included the information of d and $\mathbf{d}[u_c, v_c]$ in the output of BEV features. We propose a Depth-wise Contrastive Learning (DCL) method to encourage the model to learn the relationship between d and $\mathbf{d}[u_c, v_c]$. We assign an object ray for each object. Each point on the object ray can be mapped to a BEV feature. We take an object as example to illustrate DCL. We sample N_{pos} BEV features as positive examples and N_{neg} ones as negative ones, which are denoted as $\{f_1, f_2, \dots, f_{N_{pos}+N_{neg}}\}$ along the object ray of the object. Denote d_i as the depth of f_i and d_{gt} as the ground truth depth of the object along this object ray. The features with $|d_i - d_{gt}| \leq \delta$ are taken as positive and those with $|d_i - d_{gt}| > \delta$ are negative, where δ is a threshold to distinguish between positive and negative queries. We use this threshold to tolerate errors in depth estimation. Since the difficulty of depth estimation increases as depth increases, we set $\delta = \lambda d_{gt}$. After positive and negative features are sampled, they are fed into a box head $H_{box}(\cdot)$ and a classification head $H_{cls}(\cdot)$. Then the predictions are utilized for the auxiliary DCL task in training. We supervise the positive BEV features with the GT class of the object and “no object” for negative BEV features. We denote the box and class of the object as b and c . The contrastive loss for DCL

is formulated as follows.

$$\begin{aligned} L_{DCL} &= \sum_{i \in I_{pos}} L_{box}(H_{box}(f_i), b) + L_{cls}(H_{cls}(f_i), c) \\ &\quad + \sum_{i \in I_{neg}} L_{cls}(H_{cls}(f_i), c_{no}), \end{aligned} \quad (4)$$

where I_{pos} and I_{neg} are the sets of indices of positive BEV features and negative ones, respectively, and c_{no} is the class referring to “no object”. This contrastive loss has two purposes. First, it encourages the predicted depth d_c^i to approach to d_{gt} . Second, it enforces the model to output high classification scores for positive BEV features and low classification scores (or high score as “no object”) for negative ones, which in return help the model learn better depth-aware BEV features.

4. Experiments

4.1. Experimental settings

For others to reproduce our results, we provide details of our experiment settings in two aspects, which are datasets and implementation details.

Datasets: We conduct experiments on nuScenes dataset [1], which is a large-scale public dataset containing 1000 scenes of 20s each. It provides data from various sensors including cameras, RADAR, LiDAR, etc. Since our task is camera-based 3D detection, camera images are the only data source for us. The entire dataset is annotated at 2Hz with 40k keyframes being annotated. NuScenes re-defines mAP. Unlike the mAP in 2D detection which uses the Intersection over Union (IoU) to match predicted results and ground truth, nuScenes adopts center distance. NuScenes also define 5 true positive (TP) metrics ATE, ASE, AOE, AVE, and AAE for measuring translation, scale, orientation, velocity and attribute errors, respectively. The main metric of nuScenes is nuScenes detection score (NDS) which considers all the TP metrics. We report our results on the mAP, NDS, and all the TP metrics.

Implementation details For a fair comparison with our baseline method BEVFormer [14], we use exactly the same setting except for the methods we proposed. We adopt two backbones: ResNet101-DCN [5, 6] initialized from the FCOS3D [25] checkpoint, and VoVNet-99 [9] initialized from the DD3D [19] checkpoint. By default, we use feature maps with sizes 1/16, 1/32, and 1/32 with hidden dimensions 256. The BEV resolution is 200×200 . In Spatial Cross-Attention, each query corresponds to 4 reference points with different heights. We also adopt 6 BEV encoder layers, where each contains a Temporal Self-Attention and a Spatial Cross-Attention. Same as BEVFormer, we also adopt a deformable decoder with 6 layers and 900 queries as our box head. As for DA-SCA, we use a simple MLP with 2 Linear layers to

predict the depth map. We choose Sine Positional Encoding for both query and value. For DCL, we choose 3 positive and 3 negative examples and set the multiplier λ mentioned in section 3.4 to 0.2. We train our model with a learning rate 2×10^{-4} for 24 epochs by default. We also implement a two-stage (query selection) deformable decoder as our detection head. We find that directly using the query selection proposed by deformable DETR does not work. Hence we make some improvements. Firstly, we interpolate the BEV features from 200×200 to 50×50 because 40000 features are too many to select from. Then we select 900 features and the corresponding reference points as the initial values of queries and reference points of the detection head.

4.2. Main results

For a fair comparison with our baseline model BEVFormer and other top-performed 3D detectors, we report our performance with R101-DCN backbone on nuScenes val in Table 1, which is the most popular setting reported by most works. We also show a strong LiDAR-based method CenterPoint [30] for reference. According to the results, our single-stage DA-BEV-S improves significantly over BEVFormer by +2.2 NDS and +1.2 mAP. Compared with other models, our DA-BEV also has the best performance. BEVDet4D-Base has the same NDS with DA-BEV, but its GFLOPS is much higher than ours and the mAP is lower than ours.

To show the scalability of our model to stronger backbones, we report DA-BEV with pre-trained VoVNet-99 as the backbone on nuScenes test in Table 2. Without bells and whistles, our model exceeds the previous SOTA model BEVDepth. Our mAP is +1.2 higher than theirs. Compared with BEVFormer, DA-BEV has an improvement of +3.4 mAP and +3.1 NDS.

4.3. Ablation study

In Table 3, we show the effectiveness of each component of our model one by one. Row 1 is our baseline model BEVFormer. For rows 2 to 4, we add one component each. Simply including depth information into Spatial Cross-Attention can improve NDS by 0.8 and conducting Depth-wise Contrastive Learning can further improve NDS by 1.4. Moreover, with query selection, our model can obtain +0.6 extra improvement.

In Table 4, we give a more specific ablation on our key component Depth-wise Contrastive Learning (DCL). In the first three rows, we show the effectiveness of sampling negative examples along the same ray. For the three rows, we keep the other settings the same and only change the way of sampling negative examples. Note that we use DA-SCA for all results in Table 4. For “Random contrastive”, we choose negative examples randomly from BEV features not restricted to object rays. Meanwhile, we make sure negative features are distant from any objects. It shows that sampling depth-wise

negative examples is better than sampling negative examples randomly.

In rows 4 to 6, we show that conducting DCL on multiple BEV encoder layers is helpful. We have 6 encoder layers in total. Row 4 to 6 shows that NDS increases constantly as the number of layers conducting DCL increases.

4.4. Our method on other DETR-base models

To evaluate the applicability of our method, we also apply DA-BEV on other DETR-base models including DETR3D [27] and PETR [16]. We call the improved models as Depth-Aware DETR3D (DA-DETR3D) and Depth-Aware PETR (DA-PETR). In the following, we will show the implementation.

DA-SCA: The implementation of DA-SCA is the same as in DA-BEV. We just add (u, v, d) positional encodings to queries and image features, where the depth in image features are estimated from image features and the (u, v, d) coordinates in queries are converted from (x, y, z) coordinates in the ego-vehicle coordinate system.

DCL: DCL requires BEV features along object rays, but DETR3D and PETR do not have BEV features. Note that in BEVFormer, BEV features are probed by BEV queries from image features. Therefore, we construct reference points along object rays. Given a reference point (x, y, z) , the corresponding query Q is $Q_c + Q_p$. Q_c is a learnable embedding in DETR3D, whereas it is initialized as a zero vector in PETR. Q_p is $\text{SineEnc}(\text{Ego2cam}(x, y, z))$ for both DETR3D and PETR. The constructed queries are divided into positive queries and negative ones according to their distance with corresponding object centers and are used to query image features. After positive and negative features are queried, we can apply Depth-wise Contrastive Loss on them as in DA-BEV.

Results: Table 5 shows that our method brings +1.5 NDS and +1.9 NDS on DETR3D and PETR, respectively. The results verify our intuition that the lack of depth information is a common problem in DETR-base models such as DETR3D and PETR.

4.5. Visualization:

Fig. 4 shows a visualization of the predictions by our DA-BEV and the baseline model BEVFormer. Duplicate predictions along depth axes are reduced in Fig. 4 (b). This visualization verifies that our model can solve the ambiguity problem shown in Section 3.1. There are also some problems in predictions of DA-BEV, when the object rays of two different objects are overlapped, the object in front usually has an accurate prediction but the one behind may be missed in predictions or has a low-quality prediction. There are two potential reasons leading to this problem. Firstly, the

| Method | Modality | GFLOPs | mAP \uparrow | mATE \downarrow | mASE \downarrow | mAOE \downarrow | mAVE \downarrow | mAAE \downarrow | NDS \uparrow |
|------------------------|----------|--------|----------------|-------------------|-------------------|-------------------|-------------------|-------------------|----------------|
| CenterPoint-Voxel [30] | L | - | 0.564 | - | - | - | - | - | 0.648 |
| CenterPoint-Pillar | L | - | 0.503 | - | - | - | - | - | 0.602 |
| FCOS3D [25] | C | 2008 | 0.295 | 0.806 | 0.268 | 0.511 | 1.315 | 0.170 | 0.372 |
| DETR3D \dagger [27] | C | 1017 | 0.303 | 0.860 | 0.278 | 0.437 | 0.967 | 0.235 | 0.374 |
| BEVDet-R50 [8] | C | 215 | 0.286 | 0.724 | 0.278 | 0.590 | 0.873 | 0.247 | 0.372 |
| BEVDet-Base | C | 2963 | 0.349 | 0.637 | 0.269 | 0.490 | 0.914 | 0.268 | 0.417 |
| PETR-R50 [16] | C | - | 0.313 | 0.768 | 0.278 | 0.564 | 0.923 | 0.225 | 0.381 |
| PETR-R101 | C | - | 0.357 | 0.710 | 0.270 | 0.490 | 0.885 | 0.224 | 0.421 |
| PETR-Tiny | C | - | 0.361 | 0.732 | 0.273 | 0.497 | 0.808 | 0.185 | 0.431 |
| PETRv2 [17] | C | - | 0.401 | 0.745 | 0.268 | 0.448 | 0.394 | 0.184 | 0.496 |
| BEVDet4D-Tiny [7] | C | 222 | 0.323 | 0.674 | 0.272 | 0.503 | 0.429 | 0.208 | 0.453 |
| BEVDet4D-Base* | C | 2989 | 0.421 | 0.579 | 0.258 | 0.329 | 0.301 | 0.191 | 0.545 |
| BEVDepth-R50 | C | - | 0.351 | 0.639 | 0.267 | 0.479 | 0.428 | 0.198 | 0.475 |
| BEVDepth* | C | - | 0.412 | 0.565 | 0.266 | 0.358 | 0.331 | 0.190 | 0.535 |
| BEVFormer \dagger | C | 1304 | 0.416 | 0.673 | 0.274 | 0.372 | 0.394 | 0.198 | 0.517 |
| DA-BEV-S \dagger | C | 1312 | 0.428 | 0.633 | 0.273 | 0.331 | 0.327 | 0.188 | 0.539 |
| DA-BEV \dagger | C | 1323 | 0.433 | 0.623 | 0.271 | 0.351 | 0.309 | 0.188 | 0.545 |

Table 1. Comparison on the nuScenes *val* set. Without specification, the models use ResNet101 [6] (R101) as the backbone. \dagger denotes that the model adopts ResNet101-DCN [5] as backbone. L denotes LiDAR and C denotes camera. DA-BEV-S denotes that our model with single-stage deformable DETR as the detection head which is the same as in BEVFormer. Our model with two-stage (query selection) has better results with negligible extra computation. * denotes the model uses CBGS [34].

| Method | Modality | Backbone | mAP \uparrow | mATE \downarrow | mASE \downarrow | mAOE \downarrow | mAVE \downarrow | mAAE \downarrow | NDS \uparrow |
|------------------|----------|-----------------|----------------|-------------------|-------------------|-------------------|-------------------|-------------------|----------------|
| CenterPoint [30] | L | - | 0.674 | 0.255 | 0.235 | 0.339 | 0.233 | 0.128 | 0.718 |
| FCOS3D [25] | C | R101 | 0.358 | 0.690 | 0.249 | 0.452 | 1.434 | 0.124 | 0.428 |
| DETR3D [27] | C | V2-99 \dagger | 0.412 | 0.641 | 0.255 | 0.394 | 0.845 | 0.133 | 0.479 |
| BEVDet-Pure [8] | C | - | 0.398 | 0.556 | 0.239 | 0.414 | 1.010 | 0.153 | 0.463 |
| BEVDet-Beta | C | - | 0.422 | 0.529 | 0.236 | 0.396 | 0.979 | 0.152 | 0.482 |
| PETR [16] | C | V2-99 \dagger | 0.434 | 0.641 | 0.248 | 0.437 | 0.894 | 0.143 | 0.481 |
| PETR-e | C | Swin-T | 0.441 | 0.593 | 0.249 | 0.384 | 0.808 | 0.132 | 0.504 |
| BEVDet4D* [7] | C | - | 0.451 | 0.511 | 0.241 | 0.386 | 0.301 | 0.121 | 0.569 |
| BEVFormer [14] | C | V2-99 \dagger | 0.481 | 0.582 | 0.256 | 0.375 | 0.378 | 0.126 | 0.569 |
| PETRv2 [17] | C | V2-99 \dagger | 0.490 | 0.561 | 0.243 | 0.361 | 0.343 | 0.120 | 0.582 |
| BEVDepth* [13] | C | V2-99 \dagger | 0.503 | 0.445 | 0.245 | 0.378 | 0.320 | 0.126 | 0.600 |
| DA-BEV | C | V2-99 \dagger | 0.515 | 0.532 | 0.253 | 0.347 | 0.322 | 0.121 | 0.600 |

Table 2. Comparison on the nuScenes *test* set. L denotes LiDAR and C denotes camera. * denotes that the model uses CBGS. \dagger denotes that the VoVNet-99 (V2-99) is pre-trained on depth estimation task with extra data [19].

one behind is blocked by the one in front⁶. Secondly, in our DCL, such two objects on the same depth axis may become a negative example of each other leading to missed predictions.

⁶Note that this problem exists in both models, hence it is hard for both of them to predict the one behind accurately.

5. Conclusion

In the paper, we have revealed a problem in previous DETR-based 3D detectors, which neglect depth information in the Spatial Cross-Attention and cause a serious ambiguity problem when detecting objects. In order to solve this problem, we propose our Depth-Aware Spatial Cross-Attention (DA-SCA) to include depth information in both BEV queries

| Row | Method | Modality | mAP \uparrow | mATE \downarrow | mASE \downarrow | mAOE \downarrow | mAVE \downarrow | mAAE \downarrow | NDS \uparrow |
|-----|------------------------------|----------|----------------|-------------------|-------------------|-------------------|-------------------|-------------------|----------------|
| 1. | BEVFormer | C | 0.416 | 0.673 | 0.274 | 0.372 | 0.394 | 0.198 | 0.517 |
| 2. | Row1+DA-SCA | C | 0.420 | 0.663 | 0.269 | 0.377 | 0.359 | 0.185 | 0.525 |
| 3. | Row2+DCL | C | 0.428 | 0.633 | 0.273 | 0.331 | 0.327 | 0.188 | 0.539 |
| 4. | Row3+query selection* (Ours) | C | 0.433 | 0.623 | 0.271 | 0.351 | 0.309 | 0.188 | 0.545 |

Table 3. Effectiveness of each component. *: The implementation details of the query selection are shown in Section 4.1.

| Row | Method | Modality | mAP \uparrow | mATE \downarrow | mASE \downarrow | mAOE \downarrow | mAVE \downarrow | mAAE \downarrow | NDS \uparrow |
|-----|---------------------------------|----------|----------------|-------------------|-------------------|-------------------|-------------------|-------------------|----------------|
| 1. | Depth-wise Contrastive Learning | C | 0.428 | 0.633 | 0.273 | 0.331 | 0.327 | 0.188 | 0.539 |
| 2. | Random Contrastive Learning | C | 0.423 | 0.653 | 0.275 | 0.360 | 0.323 | 0.190 | 0.534 |
| 3. | No Contrastive Learning | C | 0.420 | 0.663 | 0.269 | 0.377 | 0.359 | 0.185 | 0.525 |
| 4. | Contrastive in first 2 layers | C | 0.422 | 0.661 | 0.274 | 0.348 | 0.334 | 0.197 | 0.530 |
| 5. | Contrastive in first 4 layers | C | 0.430 | 0.642 | 0.274 | 0.379 | 0.338 | 0.184 | 0.533 |
| 6. | Contrastive in all 6 layers | C | 0.428 | 0.633 | 0.273 | 0.331 | 0.327 | 0.188 | 0.539 |

Table 4. Effectiveness of depth-wise contrastive learning.

and image features. To help the learning of DA-SCA, DCL is proposed to help the implicit depth learning in a contrastive way. According to the experimental results, our DA-BEV obtains a remarkable improvement over the baseline and achieves a SOTA performance without bells and whistles. The ablation study verifies the effectiveness of each component of our model. Moreover, we show that our method also works when applied in DETR3D and PETR. The visualization also shows that our model effectively resolves the lack-of-depth-awareness problem in previous DETR-based 3D detectors.

Limitations and Future Work: In this paper, we improve DETR-based 3D detectors with our DA-BEV. Since depth learning is a challenging problem for all camera-based 3D detectors, we will explore to apply our method on more detectors. Moreover, we did not give a comparison of implicit depth learning with explicit one. We plan to do more exploration on the differences of the two approaches and try to combine them in the future.

References

- [1] Holger Caesar, Varun Bankiti, Alex H Lang, Sourabh Vora, Venice Erin Liong, Qiang Xu, Anush Krishnan, Yu Pan, Giancarlo Baldan, and Oscar Beijbom. nuScenes: A multi-modal dataset for autonomous driving. In *Proceedings of the IEEE/CVF Conference on Computer Vision and Pattern Recognition*, pages 11621–11631, 2020. 5
- [2] Nicolas Carion, Francisco Massa, Gabriel Synnaeve, Nicolas Usunier, Alexander Kirillov, and Sergey Zagoruyko. End-to-End Object Detection with Transformers. In *European Conference on Computer Vision*, pages 213–229. Springer, 2020. 2
- [3] Florian Chabot, Mohamed Chaouch, Jaonary Rabarisoa, Céline Teulière, and Thierry Chateau. Deep MANTA: A Coarse-to-fine Many-Task Network for joint 2D and 3D vehicle analysis from monocular image. In *Proceedings of the IEEE Conference on Computer Vision and Pattern Recognition*, pages 2040–2049, 2017. 2
- [4] Yilun Chen, Shu Liu, Xiaoyong Shen, and Jiaya Jia. DSGN: Deep Stereo Geometry Network for 3D Object Detection. In *Proceedings of the IEEE/CVF Conference on Computer Vision and Pattern Recognition*, pages 12536–12545, 2020. 1
- [5] Jifeng Dai, Haozhi Qi, Yuwen Xiong, Yi Li, Guodong Zhang,

| Method | Modality | mAP \uparrow | mATE \downarrow | mASE \downarrow | mAOE \downarrow | mAVE \downarrow | mAAE \downarrow | NDS \uparrow |
|--------------------|----------|----------------|-------------------|-------------------|-------------------|-------------------|-------------------|---------------------|
| DETR3D-R101-DCN | C | 0.347 | 0.765 | 0.268 | 0.392 | 0.876 | 0.211 | 0.422 |
| DA-DETR3D-R101-DCN | C | 0.364 | 0.756 | 0.272 | 0.373 | 0.832 | 0.216 | 0.437 (+1.5) |
| PETR-V299* | C | 0.378 | 0.746 | 0.272 | 0.488 | 0.906 | 0.212 | 0.426 |
| DA-PETR-V299* | C | 0.392 | 0.723 | 0.267 | 0.486 | 0.829 | 0.206 | 0.445 (+1.9) |

Table 5. The applicability of our method. * denotes that the VoVNet-99 (V2-99) is pre-trained on depth estimation task with extra data [19]. Note that models in this table do not use CBGS.

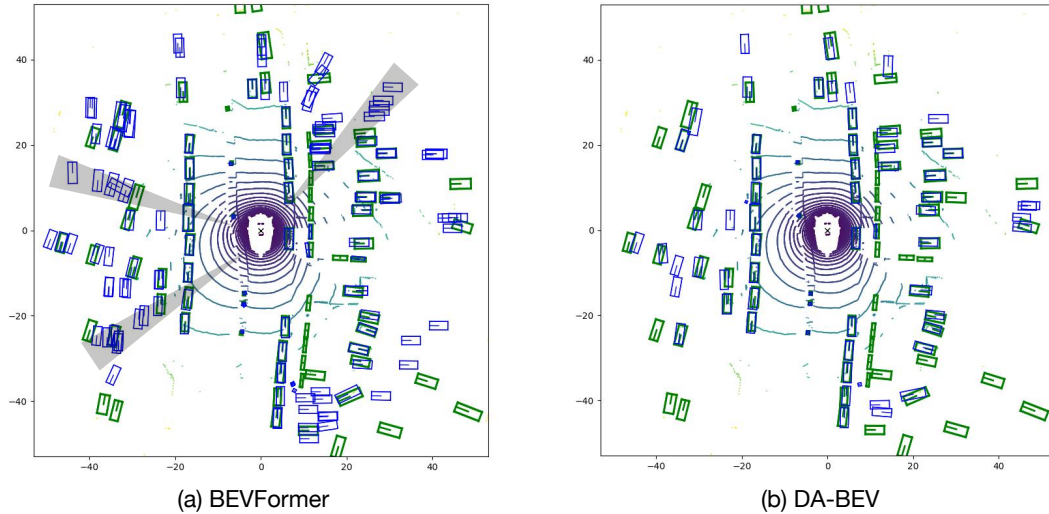


Figure 4. A visualization of predictions on BEV. Green boxes are GT boxes and blue ones are predicted ones. We use the same threshold of score > 0.1 to filter predictions for both BEVFormer and DA-BEV. (a) The predictions enclosed by shaded triangles are duplicate predictions caused by the ambiguity problem shown in Section 3.1. (b) The prediction of the same sample by DA-BEV. The problem of duplicate predictions along depth axes is alleviated.

- Han Hu, and Yichen Wei. Deformable Convolutional Networks. In *Proceedings of the IEEE International Conference on Computer Vision*, pages 764–773, 2017. 5, 7
- [6] Kaiming He, Xiangyu Zhang, Shaoqing Ren, and Jian Sun. Deep Residual Learning for Image Recognition. In *Proceedings of the IEEE Conference on Computer Vision and Pattern Recognition*, pages 770–778, 2016. 5, 7
- [7] Junjie Huang and Guan Huang. BEVDet4D: Exploit Temporal Cues in Multi-camera 3D Object Detection. *arXiv preprint arXiv:2203.17054*, 2022. 7
- [8] Junjie Huang, Guan Huang, Zheng Zhu, and Dalong Du. BEVDet: High-performance Multi-camera 3D Object Detection in Bird-Eye-View. *arXiv preprint arXiv:2112.11790*, 2021. 7
- [9] Youngwan Lee, Joong-won Hwang, Sangrok Lee, Yuseok Bae, and Jongyoul Park. An energy and gpu-computation efficient backbone network for real-time object detection. In *Proceedings of the IEEE/CVF Conference on Computer Vision and Pattern Recognition workshops*, pages 0–0, 2019. 5
- [10] Buyu Li, Wanli Ouyang, Lu Sheng, Xingyu Zeng, and Xiaogang Wang. GS3D: An efficient 3d object detection framework for autonomous driving. In *Proceedings of the IEEE/CVF Conference on Computer Vision and Pattern Recognition*, pages 1019–1028, 2019. 2
- [11] Feng Li, Hao Zhang, Shilong Liu, Jian Guo, Lionel M Ni, and Lei Zhang. DN-DETR: Accelerate DETR training by introducing query denoising. In *Proceedings of the IEEE/CVF Conference on Computer Vision and Pattern Recognition*, pages 13619–13627, 2022. 2
- [12] Peiliang Li, Xiaozhi Chen, and Shaojie Shen. Stereo R-CNN based 3d object detection for autonomous driving. In *Proceedings of the IEEE/CVF Conference on Computer Vision and Pattern Recognition*, pages 7644–7652, 2019. 2
- [13] Yin hao Li, Zheng Ge, Guanyi Yu, Jinrong Yang, Zengran Wang, Yukang Shi, Jianjian Sun, and Zeming Li. BEVDepth: Acquisition of reliable depth for multi-view 3d object detection. *arXiv preprint arXiv:2206.10092*, 2022. 1, 2, 7
- [14] Zhiqi Li, Wenhai Wang, Hongyang Li, Enze Xie, Chonghao Sima, Tong Lu, Qiao Yu, and Jifeng Dai. BEVFormer: Learning Bird’s-Eye-View Representation from Multi-Camera Images via Spatiotemporal Transformers. *arXiv preprint arXiv:2203.17270*, 2022. 1, 2, 5, 7
- [15] Shilong Liu, Feng Li, Hao Zhang, Xiao Yang, Xianbiao Qi, Hang Su, Jun Zhu, and Lei Zhang. DAB-DETR: Dynamic Anchor Boxes are Better Queries for DETR. In *International Conference on Learning Representations*, 2021. 2
- [16] Yingfei Liu, Tiancai Wang, Xiangyu Zhang, and Jian Sun. Petr: Position embedding transformation for multi-view 3d object detection. *arXiv preprint arXiv:2203.05625*, 2022. 1, 2, 3, 6, 7
- [17] Yingfei Liu, Junjie Yan, Fan Jia, Shuailin Li, Qi Gao, Tiancai Wang, Xiangyu Zhang, and Jian Sun. PETRv2: A Unified Framework for 3D Perception from Multi-Camera Images. *arXiv preprint arXiv:2206.01256*, 2022. 7
- [18] Arsalan Mousavian, Dragomir Anguelov, John Flynn, and Jana Kosecka. 3D Bounding Box Estimation Using Deep Learning and Geometry. In *Proceedings of the IEEE conference on Computer Vision and Pattern Recognition*, pages 7074–7082, 2017. 2
- [19] Dennis Park, Rares Ambrus, Vitor Guizilini, Jie Li, and Adrien Gaidon. Is Pseudo-Lidar needed for Monocular 3D Object detection? In *Proceedings of the IEEE/CVF International Conference on Computer Vision*, pages 3142–3152, 2021. 1, 2, 5, 7, 8

- [20] Dennis Park, Rares Ambrus, Vitor Guizilini, Jie Li, and Adrien Gaidon. Is pseudo-lidar needed for monocular 3d object detection? In *Proceedings of the IEEE/CVF International Conference on Computer Vision*, pages 3142–3152, 2021. [2](#)
- [21] Rui Qian, Xin Lai, and Xirong Li. 3d object detection for autonomous driving: a survey. *Pattern Recognition*, page 108796, 2022. [2](#)
- [22] Cody Reading, Ali Harakeh, Julia Chae, and Steven L Waslander. Categorical depth distribution network for monocular 3d object detection. In *Proceedings of the IEEE/CVF Conference on Computer Vision and Pattern Recognition*, pages 8555–8564, 2021. [1](#), [2](#)
- [23] Xuepeng Shi, Qi Ye, Xiaozhi Chen, Chuangrong Chen, Zhixiang Chen, and Tae-Kyun Kim. Geometry-based distance decomposition for monocular 3d object detection. In *Proceedings of the IEEE/CVF International Conference on Computer Vision*, pages 15172–15181, 2021. [2](#)
- [24] Ashish Vaswani, Noam Shazeer, Niki Parmar, Jakob Uszkoreit, Llion Jones, Aidan N Gomez, Łukasz Kaiser, and Illia Polosukhin. Attention is All You Need. *Advances in neural information processing systems*, 30, 2017. [3](#)
- [25] Tai Wang, Xinge Zhu, Jiangmiao Pang, and Dahua Lin. Fcos3d: Fully convolutional one-stage monocular 3d object detection. In *Proceedings of the IEEE/CVF International Conference on Computer Vision*, pages 913–922, 2021. [1](#), [5](#), [7](#)
- [26] Yan Wang, Wei-Lun Chao, Divyansh Garg, Bharath Hariharan, Mark Campbell, and Kilian Q Weinberger. Pseudo-lidar from visual depth estimation: Bridging the gap in 3d object detection for autonomous driving. In *Proceedings of the IEEE/CVF Conference on Computer Vision and Pattern Recognition*, pages 8445–8453, 2019. [1](#), [2](#)
- [27] Yue Wang, Vitor Campagnolo Guizilini, Tianyuan Zhang, Yilun Wang, Hang Zhao, and Justin Solomon. DETR3D: 3D Object Detection from Multi-view Images via 3D-to-2D Queries. In *Conference on Robot Learning*, pages 180–191. PMLR, 2022. [1](#), [2](#), [3](#), [4](#), [6](#), [7](#)
- [28] Xinshuo Weng and Kris Kitani. Monocular 3d object detection with pseudo-lidar point cloud. In *Proceedings of the IEEE/CVF International Conference on Computer Vision Workshops*, pages 0–0, 2019. [1](#)
- [29] Bin Xu and Zhenzhong Chen. Multi-level fusion based 3d object detection from monocular images. In *Proceedings of the IEEE Conference on Computer Vision and Pattern Recognition*, pages 2345–2353, 2018. [1](#)
- [30] Tianwei Yin, Xingyi Zhou, and Philipp Krahenbuhl. Center-based 3d object detection and tracking. In *Proceedings of the IEEE/CVF Conference on Computer Vision and Pattern Recognition*, pages 11784–11793, 2021. [6](#), [7](#)
- [31] Yurong You, Yan Wang, Wei-Lun Chao, Divyansh Garg, Geoff Pleiss, Bharath Hariharan, Mark Campbell, and Kilian Q Weinberger. Pseudo-lidar++: Accurate depth for 3d object detection in autonomous driving. *arXiv preprint arXiv:1906.06310*, 2019. [2](#)
- [32] Hao Zhang, Feng Li, Shilong Liu, Lei Zhang, Hang Su, Jun Zhu, Lionel M Ni, and Heung-Yeung Shum. DINO: DETR with Improved DeNoising Anchor Boxes for End-to-End Object Detection. *arXiv preprint arXiv:2203.03605*, 2022. [2](#)
- [33] Xingyi Zhou, Dequan Wang, and Philipp Krähenbühl. Objects as points. *arXiv preprint arXiv:1904.07850*, 2019. [1](#)
- [34] Benjin Zhu, Zhengkai Jiang, Xiangxin Zhou, Zeming Li, and Gang Yu. Class-balanced grouping and sampling for point cloud 3d object detection. *arXiv preprint arXiv:1908.09492*, 2019. [7](#)
- [35] Xizhou Zhu, Weijie Su, Lewei Lu, Bin Li, Xiaogang Wang, and Jifeng Dai. Deformable DETR: Deformable Transformers for End-to-End Object Detection. In *International Conference on Learning Representations*, 2020. [2](#), [3](#)